Original Article

Institution of MECHANICAL ENGINEERS
Journal of RAIL AND RAPID TRANSIT

Proc IMechE Part F:
J Rail and Rapid Transit
2014, Vol. 228(6) 590–602

DOI: 10.1177/0954409714529558
pif.sagepub.com
SAGE

Finite element modeling and validation of the fastening systems and concrete sleepers used in North America

Zhe Chen[1], Moochul Shin[2], Sihang Wei[1], Bassem Andrawes[1] and Daniel A Kuchma[1]

Abstract

Significant increases in rail loads, as well as growing interest in providing higher-speed passenger rail services, is placing new and increasing existing demands on fastening systems and concrete sleepers. Consequently, there is a strong need to better understand the response of fastening systems and concrete sleepers to these significantly increased demands. This paper presents an experimentally validated three-dimensional (3D) finite element (FE) model of a fastening system and concrete sleeper that can be used to study and improve the design and performance of these systems. In this 3D FE model, the following mechanisms that are critical to the performance of fastening systems and concrete sleepers are included: frictional interaction between components of the fastening system; interaction between shoulders and concrete; and the plastic behavior of each component in the system. The FE model is validated using laboratory experimental tests, in which a lateral load is applied to a single concrete sleeper with two sets of fastening systems. The validated FE model is used to analyze the sleeper/fastening system under different loading scenarios involving various vertical and lateral load combinations. Both component stress and system deflection of the model are analyzed to investigate the system performance at the component and system levels. The results of the study show that FE modeling can be used to investigate the complex behavior of fastening systems and concrete sleepers.

Keywords

Pre-stressed concrete sleeper, fastening systems, loading path, finite element modeling, laboratory testing, model validation

Date received: 14 August 2013; accepted: 17 January 2014

Introduction

In North America, there is an increasing demand on the railroad infrastructure and its components due to ever heavier axle loads on freight trains and interest in running higher-speed passenger trains on predominantly freight lines. The dominant design approach for concrete sleeper and fastening systems are iterative, empirical, and based on speed and traffic to meet the design load in the American Railroad Engineering and Maintenance-of-Way Association (AREMA)'s Recommended Practices.[1] To ensure that freight and passengers are safely transported and the necessary track geometry is maintained, further investigation into the behavior and interaction of the concrete sleeper and fastening system is needed. In addition, a mechanistic design approach based on a detailed structural analysis would be beneficial for infrastructure manufacturers; such an approach is expected to reduce costs on overdesigned parts, increase longevity, as well as reducing maintenance requirements.

Researchers have performed some innovative studies on the modeling of concrete sleepers and fastening systems. To investigate the dynamics of vehicles and track structures, mathematical models have been built to represent this system. For example, Frohling[2] proposed a mathematical model that related track deterioration to wheel loads and spatially varying

[1]Department of Civil and Environmental Engineering, University of Illinois at Urbana-Champaign, USA
[2]Department of Civil and Environmental Engineering, Western New England University, USA

Corresponding author:
Bassem Andrawes, Department of Civil and Environmental Engineering, University of Illinois at Urbana-Champaign, 3122 Newmark Civil Engineering Laboratory, MC-250, 205 North Mathews Avenue, Urbana, IL 61801, USA
Email: andrawes@illinois.edu

track stiffness levels. In addition, several studies have used finite element (FE) analysis to gain a better understanding of the behavior of concrete sleepers and fastening systems, and this work has provided some insight into the application of the FE technique.[3-6] For example, Yu and Jeong[4] conducted three-dimensional (3D) FE analyses on a pre-stressed concrete sleeper and ballast. A pre-stress and a direct uniaxial static rail-seat loading were applied in the model. A quarter-symmetric model was used to compare the performance of the concrete sleeper at different support conditions. The model assumed a perfect bond between the concrete and strand; this ignores the possibility of slip of strands and thereby causes the effect of the pre-stressing to be magnified. Yu et al. conducted FE analyses that included an improved 3D model of the concrete sleeper with ballast and subgrade support.[3] In this model the interaction between concrete and strand was modeled as a cohesive element that is incorporated between them to simulate a force/slip relationship based on experimental data.[7] Using the model, several factors that could affect the performance of the concrete sleeper were investigated including strand pattern and different loading patterns. A failure analysis of a heavy-haul freight track was developed by Gonzalez-Nicieza et al.[8] In that analysis, both a single-sleeper model and a multi-sleeper model were built that were based on data collected in a field investigation; the model was subsequently used to investigate the cause of sleeper cracking. However, the model assumed elastic material properties for all the track components, and the fastening system was ignored. Rezaie et al.[9] have also built an FE model of a concrete sleeper to investigate the cause of longitudinal cracks in sleepers. Nonlinear material properties were defined in the model and the study mainly focused on the response of the concrete sleeper to an increasing Rawlplug pressure rather than wheel load. Kaewunruen and Remennikov[10] presented a dynamic FE model of a concrete sleeper and used it to investigate the sleeper's transient response under an impact load. However, the model only included the concrete sleeper and all other components were replaced by springs.

Based on the presented literature review, it is evident that there is still significant room for improvement in FE modeling of concrete sleepers and fastening systems. As part of a large research project funded by the Federal Railroad Administration (FRA) that is aimed at further understanding and improving the design of concrete sleepers and fastening systems, this study used a detailed FE model to investigate the performance of concrete sleepers and fastening systems. The created model can serve as a tool that allows theoretical comparison with the results from laboratory and field testing as well as a tool to perform parametric studies of component material properties and geometric dimensions. These studies were conducted to serve the primary goal of developing new mechanistic design criteria for concrete sleeper and fastening systems able to satisfy the ever-increasing loading demands in North America. In this paper, a detailed 3D model of the concrete sleeper and fastening system is presented under various loading scenarios including a pre-stress force, vertical wheel loading and lateral wheel loading at different levels. This model is an improvement on existing models in that it includes the components of fastening system based on the manufacturer's design, and thus it is able to provide detailed comparisons of fastening systems with different designs. The FE program ABAQUS[11] is used to develop the model. Nonlinear material properties are defined for the components. Frictional interactions are defined between different components. The FE model is validated and calibrated using laboratory test data that includes a single sleeper and two sets of fastening systems. A study is conducted using the model on the impact of the lateral/vertical loading ratio on the load path (from the loading points to the sleeper) and the stress state in all components of the system.

Modeling configuration

System description

Figure 1 presents the layout of the fastening system considered in the FE model. As shown, the fastening system is connected to the concrete sleeper and transmits the load from the rail to the concrete surface; thus maintaining a uniform track geometry. Fastening systems of various designs are used in practice, and different systems consist of different components. The fastening system modeled in this paper includes embedded iron shoulders, clips, nylon insulators, and a two-part rail pad assembly consisting of a resilient polyurethane pad for load attenuation and a nylon abrasion plate to mitigate abrasion of the concrete. The embedded shoulder provides support for other components. The clip is elastically deformed and then inserted into the shoulder to prevent longitudinal and lateral displacement of the rail. The insulator is placed between the clip and rail and between the rail base and shoulder to provide electrical isolation between the two rails. Two sets of fastening systems, which were placed on each side of the rail flange, are included in the model. The pre-stressed concrete sleeper is simplified into a concrete block, as the laboratory test was focused on the performance of the fastening system, and a pre-stressed concrete sleeper was mainly used as a support. In the working environment, the wheel loading can be divided into a vertical load, which is applied on the head of the rail, and a lateral load that is pointing from the gauge side to the field side. In this model the simplified geometries of all the components are used.

The component models of the fastening system are shown in Figure 2.

For all the components, a 3D linear hexahedral element was used in the meshing. A 3D hexahedral element has eight nodes, and every node has three translational degrees of freedom. In total, the model included 24,589 elements, and different mesh densities were assumed for different components. Based on the result of a mesh sensitivity test, a dense mesh was defined in the clip due to the clip behavior being sensitive to the mesh density, and a relatively coarse mesh was defined in the rail as little difference was observed in its behavior using a finer mesh.

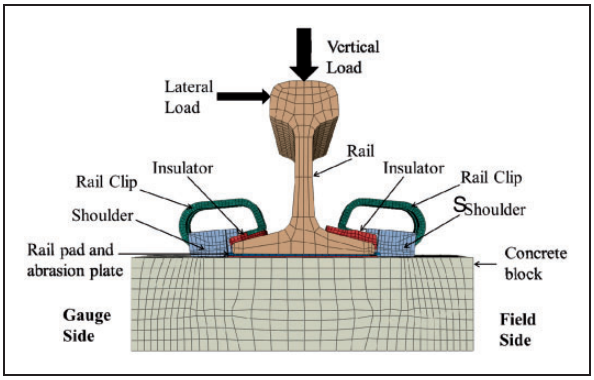

Figure 1. Layout of the 3D FE model of the concrete sleeper and fastening system.

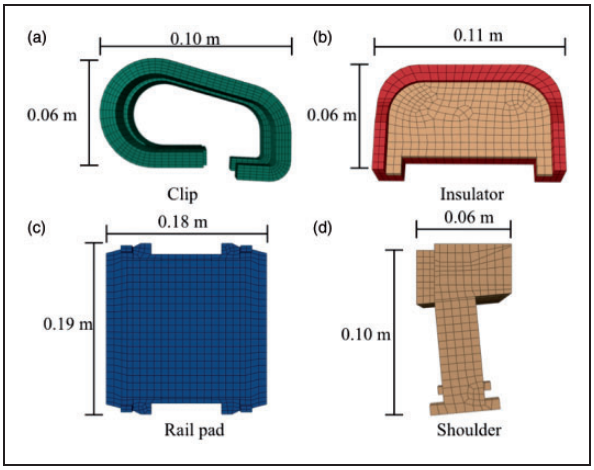

Figure 2. Components of the FE model: (a) clip; (b) insulator; (c) rail pad; and (d) shoulder.

Constitutive relationships

A plasticity model was used to define the material properties of the damaged concrete.[11] In this material model, two main failure mechanisms were considered, namely, tensile cracking and compressive crushing. As shown in Figure 3, under uniaxial tension, concrete first goes through a linear-elastic stage, and when stress reaches the cracking stress it follows a softening stress–strain relationship. Under uniaxial compression the initial response is linear until the yielding stress is reached. In the plastic stage the response is first characterized by strain hardening and then strain softening after reaching its compressive ultimate stress. As cyclic loading was not included in the current model, the two damage parameters (d_t and d_c in Figure 3) related to unloading stiffness were not defined.

For all the components of the fastening system, including shoulder, clip, rail pad, abrasion plate, insulator as well as the rail, a two-stage material property model was defined. In the initial stage, the material follows a linear-elastic relationship. The plastic stage consists of a strain-hardening range followed by a strain-softening range. The material properties for the components of the model of the concrete sleeper and fastening system are summarized in Table 1.

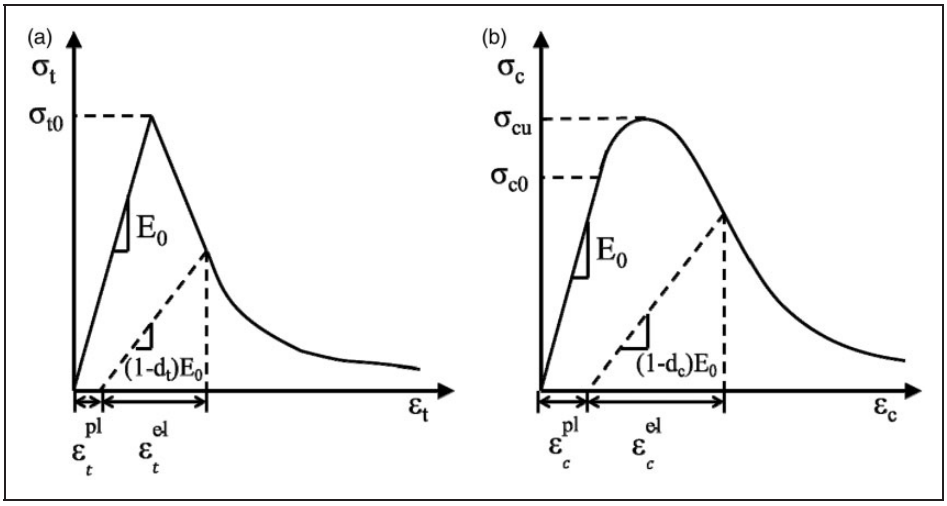

Figure 3. Stress–strain relationship in concrete in (a) tension and (b) compression.

Component interactions

Interactions between various components of the fastening system were defined with contact pairs in ABAQUS.[11] A master surface and a slave surface of different mesh densities were identified. Some of the coefficient of friction (COF) values were obtained in a series of large-scale abrasion resistance tests recently performed at the University of Illinois at Urbana-Champaign,[12] and others were taken from the literature.[13] The COF values defined in the model are listed in Table 2, and the locations of the interactions are shown in Figure 4. To allow a focus on the interaction between concrete and fastening system, the concrete sleeper was simplified into a concrete block (0.42 m (length) × 0.23 m (width) × 0.11 m (depth)). Pre-stressed strands were not modeled and the effect of the pre-stressing of the concrete was considered by applying a predefined stress field in the concrete that resulted in a uniform lateral compressive stress of 6.21 MPa (900 psi). This value was determined after reviewing the effect of applying a pre-stressing force of 31.1 kN (7000 lb) to each strand around a shoulder using a full-scale concrete sleeper model.

The interaction between the concrete block and shoulder inserts is difficult to simulate due to it being related to multiple surfaces that can result in a tensile stress between the two components. In this model, the cohesive stress between concrete and shoulder inserts was neglected. Slots based on the geometry of the shoulder inserts were cut into the concrete and interaction pairs were defined between the internal surfaces of the concrete and the surfaces of the shoulder inserts; hence, only compressive interactions were considered in the model. Based on the manufacturer's design, the gap between the insulator and shoulder could not be explicitly determined, as the position relationship is not described in detail. In the 3D model the gap was set to be 0.127 mm (0.005 inch), as in relative sliding between concrete and abrasion plate was observed in the performed experiments, however, the support of the shoulder prevents large relative displacements. This is important because the interaction between the shoulder and insulator considerably affects the load path through the fastening system under lateral loading conditions. Due to this gap, lateral resistance first results from the friction between the abrasion plate and concrete and an uneven clamping force due to rail sliding. As the insulator and shoulder came in contact, the resistance from the shoulder shares part of the loading.

Boundary conditions and analysis sequence

In the model, boundary conditions were applied at the lateral and bottom surfaces of the concrete to provide lateral and vertical resistances for the system. These boundary conditions were designed so as to simulate the support conditions in the laboratory tests used to validate the FE model, as will be discussed later. In addition, temporary boundary conditions were applied to all the components in order to stabilize the system; they were later removed under loading.

Table 2. COF values used in the FE model.

Component	Frictional interaction	COF value
Pad	Pad-frame	0.3
	Pad-rail	0.3
Abrasion frame	Frame-concrete	0.3
Insulator	Insulator-rail	0.15
	Insulator-clip	0.15
	Insulator-shoulder	0.15
Shoulder	Shoulder-clip	0.5

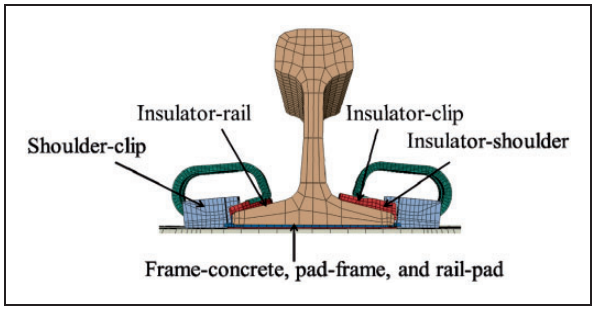

Figure 4. Locations of the interactions between components.

Table 1. Material properties of the components of the model.

Component	Young's modulus (GPa)	Poisson's ratio	Yielding strength (MPa)	Ultimate/peak strength (MPa)	Cracking strength (MPa)
Concrete	30.0	0.2	NA	48.3	5.5
Clip	158.6	0.29	1261.8	1393.2	
Rail	206.9	0.3	1034.3	1034.3	
Insulator	3.0	0.39	64.1	84.8	
Rail pad	0.1	0.49	8.3	35.9	
Abrasion plate	3.0	0.39	64.1	84.8	

Multiple analysis steps were defined to apply different types of loading. In the first step, a pre-stress was applied to the concrete with a predefined stress field and interactions were initiated with temporary loadings. In the second step, pressure loadings were applied on the surface of the toe of the clips to simulate the process of clip lifting. A load of 15.6 kN (3.5 kips) was applied to create a large deformation prior to releasing the toe of the clip in the following step. In the third step, the pressure on the toe of the clip was gradually decreased with time as the clips were slowly released onto the insulator to apply the designed clamping force. In the fourth step, a vertical load was applied on the railhead, and in the fifth step, a lateral load was introduced. The magnitudes of the vertical and lateral loads were determined based on the test loading scenario or track loading condition, which is discussed in their corresponding sections. The general loading procedure of the model is also shown in Figure 5.

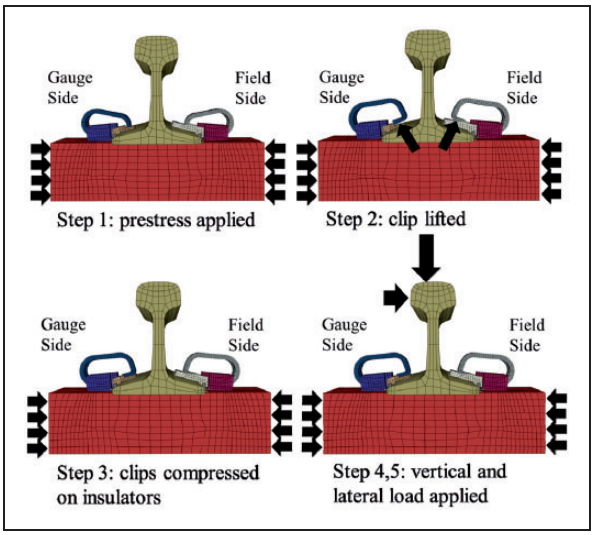

Figure 5. Loading steps of the FE model.

Model validation

Laboratory test setup

To examine the load path through the fastening system and validate the FE model, laboratory testing was conducted on a pre-stressed concrete sleeper and two sets of fastening systems. As shown in Figure 6, during the test the concrete sleeper was placed on a steel frame, and a thin wooden pad was inserted between the bottom surface of the tie and the loading frame. Two sets of fastening systems and two segments of 0.61 m (24 inches) long rail were installed on the sleeper. Most the measurement instruments were placed on the left rail seat; however, a load cell was placed between the portable track loading fixture (PTLF) loading head and the rail segment on the right side to record the applied lateral load. By using the PTLF, the lateral load can be applied to the rail web, and the response of the system was measured during the test. To achieve this, multiple sensors were used including strain gauges and potentiometers.

Loading procedure

To compare with the FE analysis results, the PTLF was used to apply a lateral load to the two rails at the rail web. The lateral force was applied via a hand-powered hydraulic jack. The capacity of the PTLF was 22.2 kN (5 kips), and a 10 kN (2.2 kips) lateral load was applied to the rail in the test. The location of the contact point between the PTLF loading head and the rail web was at the centerline of the rail seat and 1 inch higher than the top surface of the clips.

Test measurements

In this laboratory test, the sensing instruments included strain gauges, linear potentiometers and a load cell. As shown in Figure 7, strain gauges in the vertical direction were attached to the surface of the

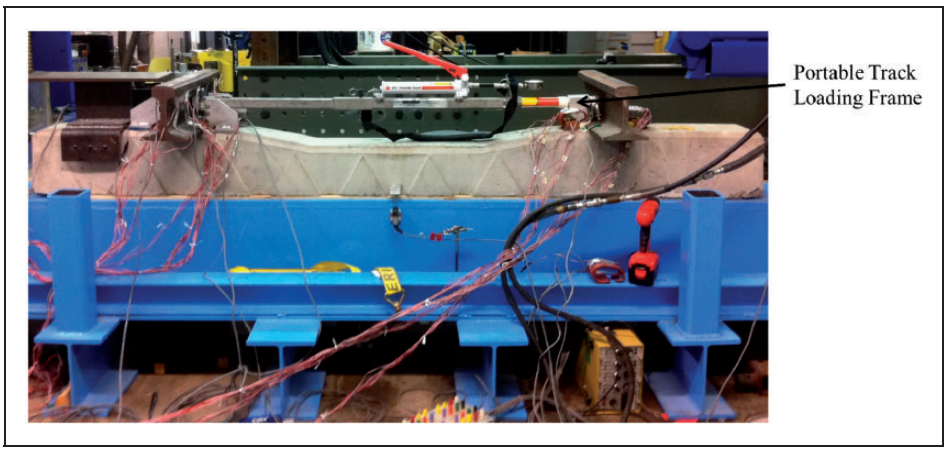

Figure 6. Laboratory test setup of the concrete sleeper and fastening systems.

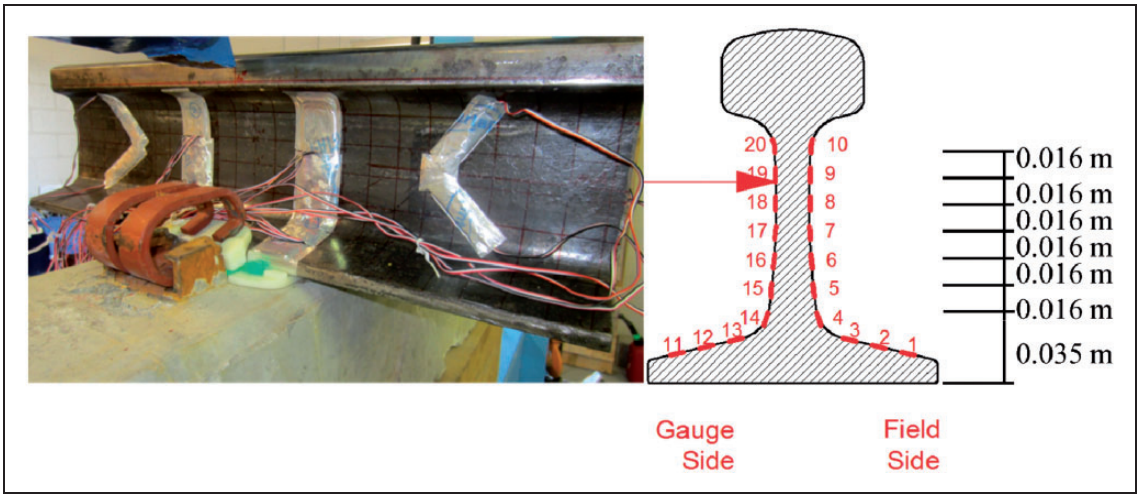

Figure 7. The rail used in the laboratory test and attached strain gauges.

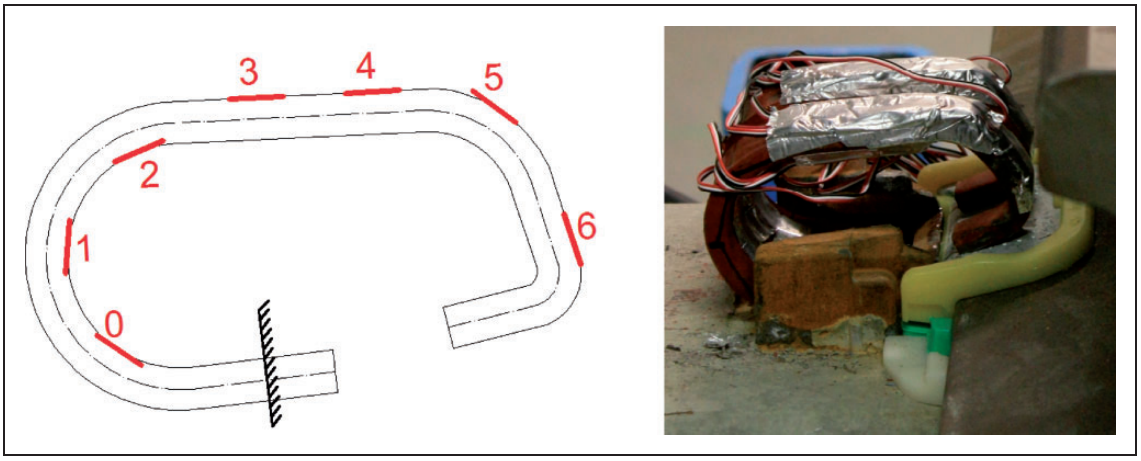

Figure 8. Layout of the strain gauges attached to the clips.

rail web, and they were labeled with numbers based on their relative height. Two lines of strain gauges were attached to each side of the rail, and in each line there were 10 strain gauges. Strain measurement from gauges 4 to 10 and 14 to 20 are used in the comparisons with the FE model in later sections of this paper. The strain gauges were attached to measure the vertical strain of the rail due to lateral loading.

During the test, seven strain gauges were attached to each toe of the clips. The instrumented clips were installed at both field and gauge sides of the rail seat. The positions of the strain gauges are marked with red lines in Figure 8, and were numbered 0 to 6. Along the central line of the clip (dashed line in Figure 8), the distance from the fixed end to the strain gauge section increased from 1 inch (gauge 0) to 7 inches (gauge 6).

As shown in Figure 9, five linear potentiometers were used to measure the displacement of the rail under lateral loadings, and they were all fixed with a steel frame connected to the sleeper. Potentiometers 1 to 4 measured the vertical displacement at the rail base, while potentiometer 5 measured the lateral displacement at the railhead. The positions of potentiometers 1 to 4 are shown in Figure 9, and potentiometer 5 was aligned with the applied lateral load at a height of 0.165 m from the rail base.

Comparison between model output and test measurement

Based on the laboratory test setup, the FE model described earlier was slightly modified. As shown in Figure 10, a steel cube was introduced in contact with the rail web to represent the loading head of the PTLF. This is done because the surface of the loading head and that of the rail web were not parallel due to the cant of the rail seat, and the contact stress concentration can be simulated by the interaction between the loading head and the rail web.

The comparison between the numerical FE model results and test measurements of the vertical strain on the field side and gauge side of the rail web are shown in Figures 11 and 12, respectively. The vertical strain gauges attached to the rail web at different heights were given numbers, and a sketch showing the relative height of the lateral load and strain gauges is included

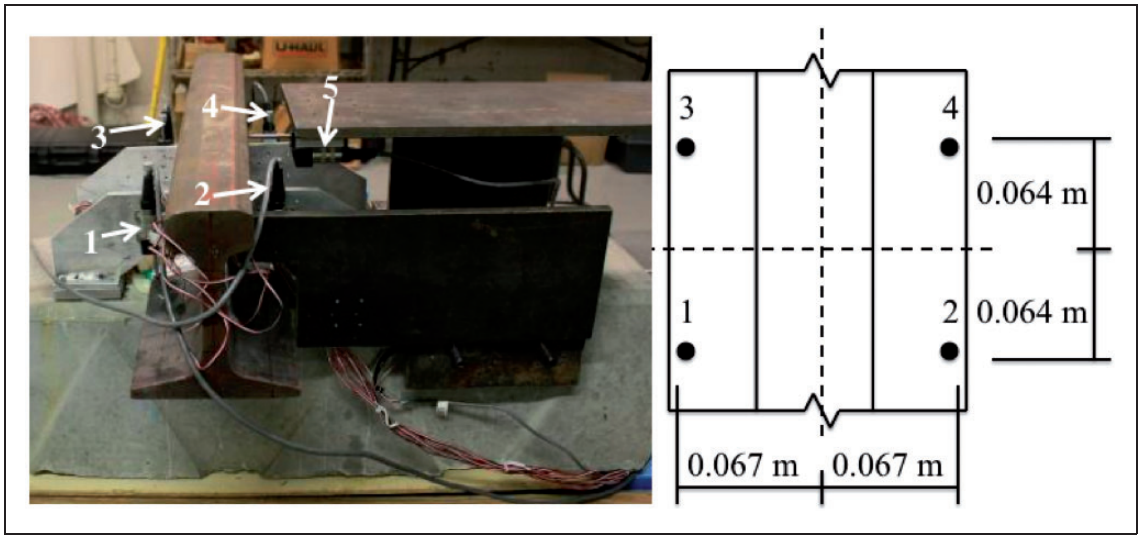

Figure 9. Layout of the linear potentiometers used to measure the rail displacement.

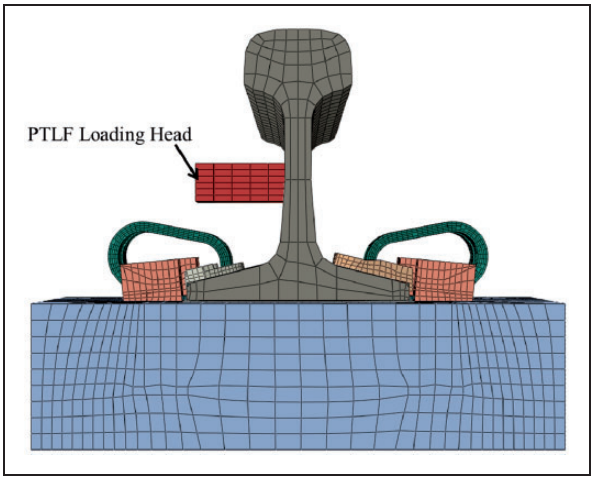

Figure 10. The FE model modified in response to the laboratory test setup.

in Figures 11 and 12. Since the PTLF applied the lateral load at a height close to strain gauge 18, the strain reading from gauges 8 to 10 at the field side and 18 to 20 at the gauge side are very small. For the strain measured from gauges 5 to 7 and 15 to 17, it was negative at the field side and positive at the gauge side, and larger strain measurements were observed at lower positions. This result clearly indicates bending behavior of the rail, which is similar to the behavior of a cantilever beam, where the field side of the rail web is in compression and the gauge side in tension.

In Figures 11 and 12, every set of strain comparisons (model output and test measurement) are shown using the same line type. The vertical rail strains increase linearly with lateral load, and generally good agreement is observed between the numerical and experimental results. Different degrees of agreement in strain are observed at different positions. Close to the middle of the rail web (strain gauges 6, 7 and 8) where the surface is relatively flat, a better agreement is observed than other positions close to the railhead or rail base, where the rail surface is relatively curved.

In addition, the height of the lateral load was between strain gauges 18 and 19 (gauge side) and strain gauges 8 and 9 (field side), and it can be observed that in the model output, the sign of the strain changes at higher positions (strain gauges 9 and 10). This change is due to the fact that the rail has a considerable length in the longitudinal direction, and as a result it acts like a combination of a beam and a plate. The geometry of the rail was correctly captured in the model, and the test measurement of rail strain on the field side agreed with model output, that the sign of rail strain changed at higher positions than the load.

The comparisons between the numerical and experimental strain results of gauge- and field-side clips are shown in Figures 13 and 14, respectively. In each set of comparisons, the model output was compared with the two strain gauge measurements at the same position of the two toes. Some gauges were damaged and they are not shown in the comparison. To focus on the behavior of the clip after installation, the strain data was compared after initialization, so that a zero strain was observed before the load was applied. It can be observed that the strain measurements at the same position of the two toes are not identical; this suggests that the behaviors of the two clip toes could be different. The strain prediction based on the FE model is close to the strain measurement. In both the model output and test measurement, the clip surface strain increases linearly with lateral load, and minor nonlinear behavior can be observed in the test measurement. The nonlinear behavior could be due to the complexity in post-processing and clip installation processes. It was confirmed by the manufacturer that the clip becomes hardened by large deflections, and this process was

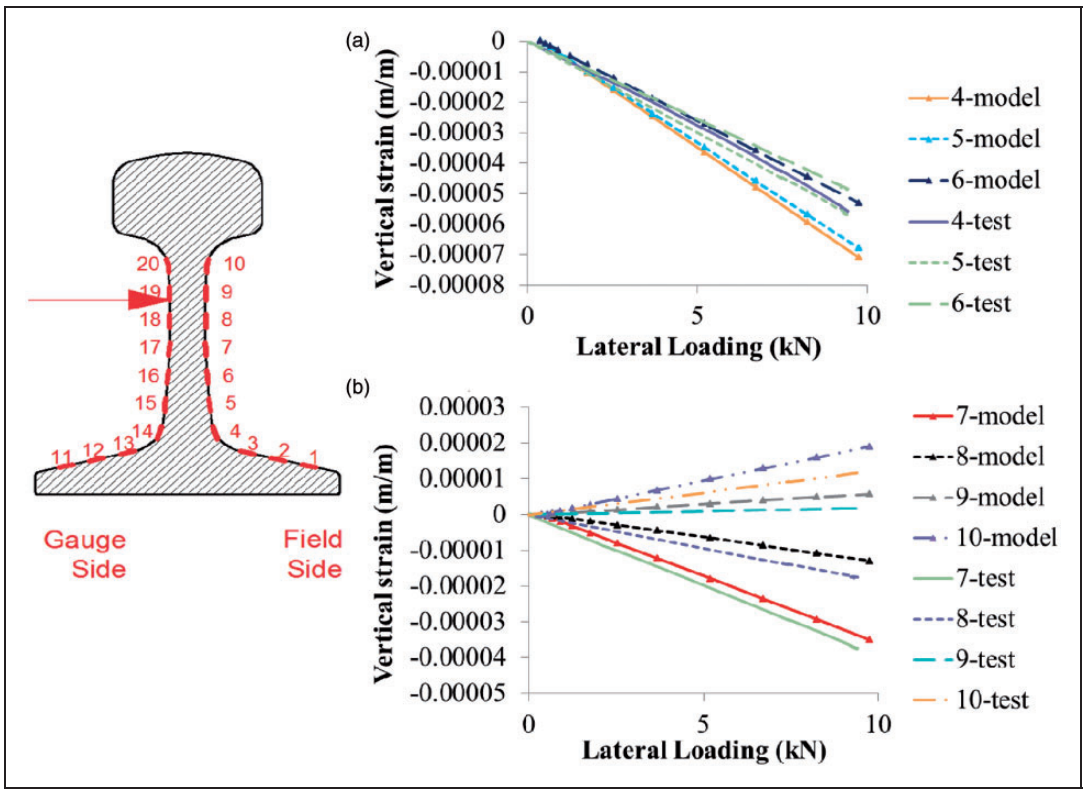

Figure 11. Comparison of model and test values of the field-side rail vertical strain. (a) Comparison for strain gauge 4–6, and (b) Comparison for strain gauge 7–10.

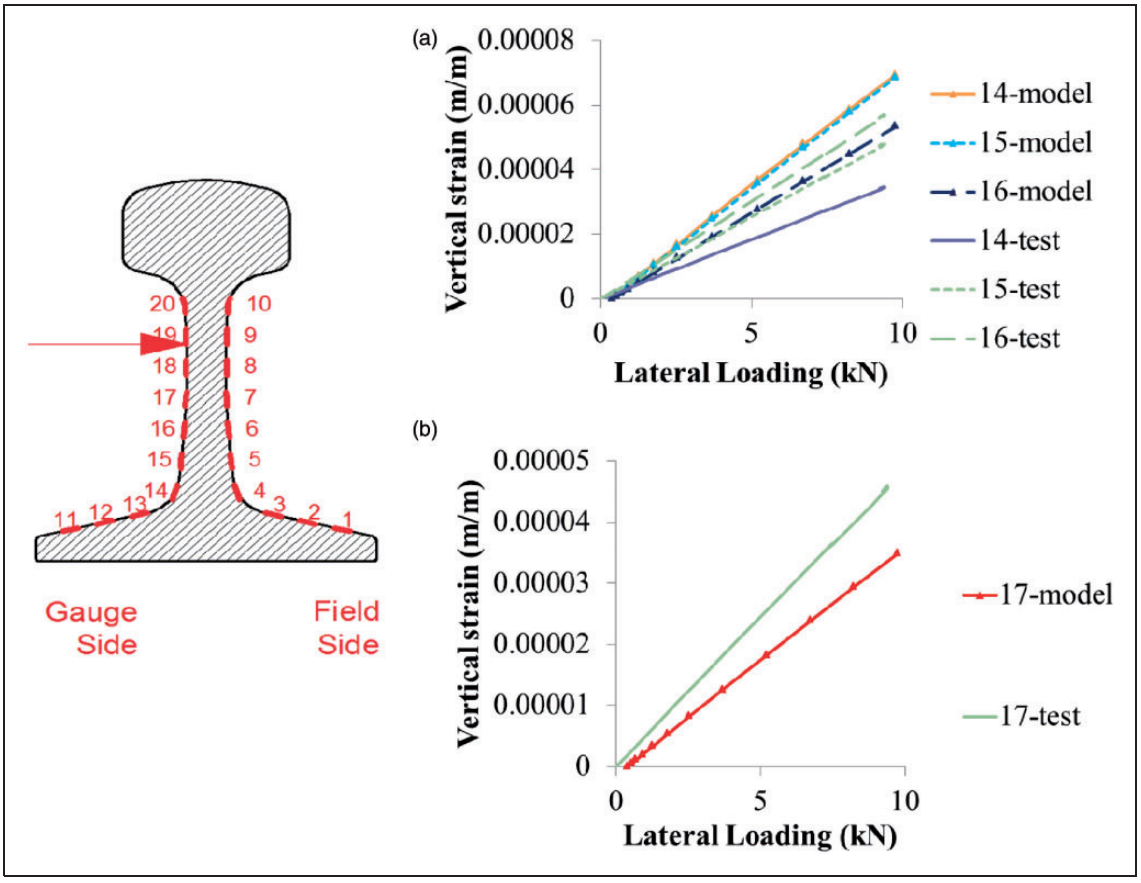

Figure 12. Comparison of model and test values of the gauge-side rail vertical strain. (a) Comparison for strain gauge 14–16, and (b) Comparison for strain gauge 17.

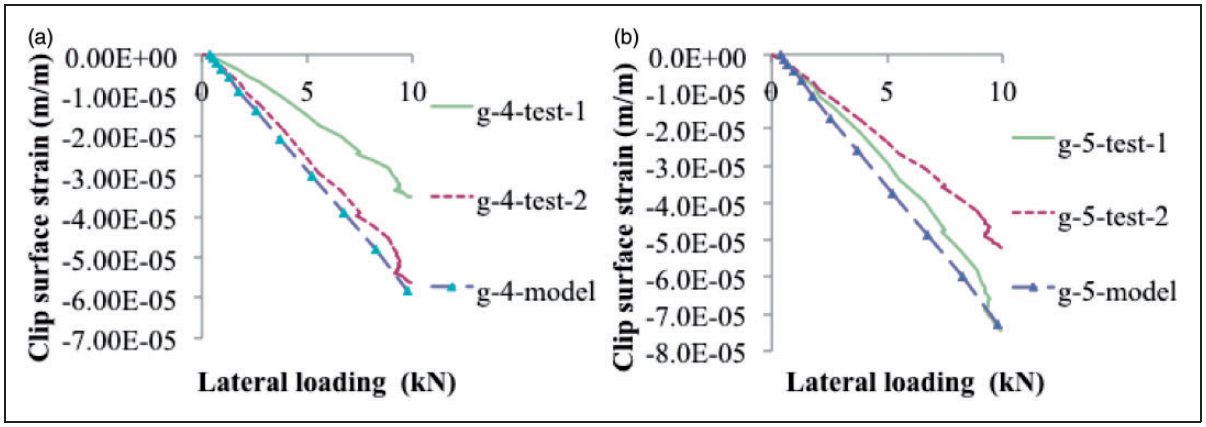

Figure 13. Comparison of model and test values of the gauge-side clip strain. (a)Comparison for strain gauge 4, and (b) Comparison for strain gauge 5.

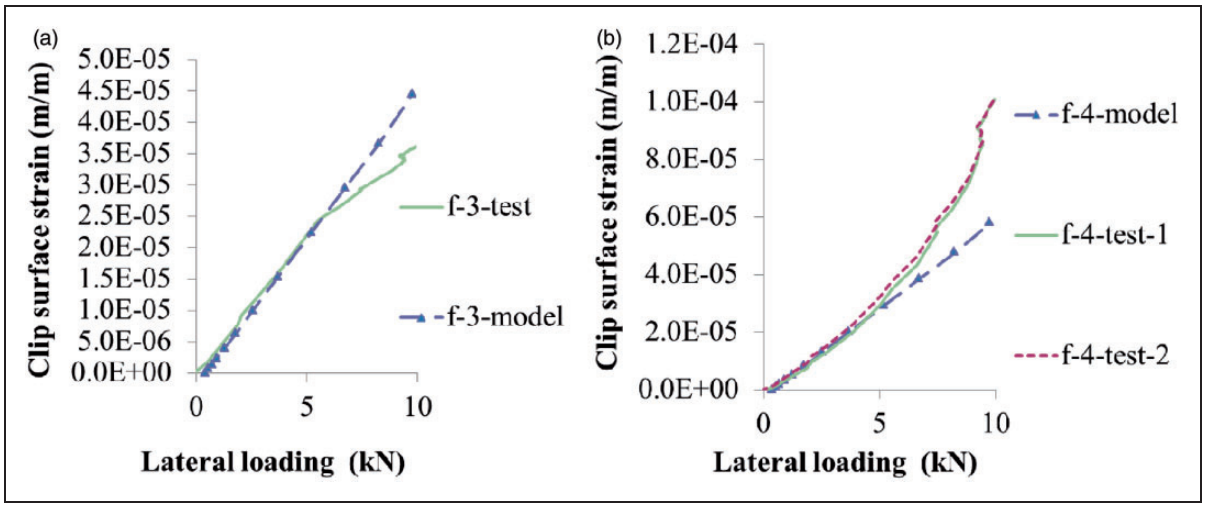

Figure 14. Comparison of model and test values of the field-side clip strain. (a) Comparison for strain gauge 3, and (b) Comparison for strain gauge 4.

not captured in the model. In addition, the clips were installed with a hammer and a lever, and this manual installation process can introduce some effects that are hard to capture in the FE model. Moreover, the surface strain on the clip is sensitive to the position of the strain gauges, and minor differences in these positions between the FE model and the test setup could also result in an error.

In addition, under an increasing lateral load, an increasing compressive strain was observed on all the strain measurements on the gauge-side clip, whereas a decreasing compressive strain was observed on all the strain measurement on the field-side clip. As the gauges were on the exterior surface of the clips, it was noticed that under lateral loading the clamping force on the gauge side was increasing whereas the clamping force on the field side was decreasing. This was validated through further investigations into the interaction between the clips and the insulators in the model. Theoretically, this effect occurs due to the rail base on the gauge side being lifted up during the rotation of the rail, this induces a larger deflection of the clip and larger clamping force. In contrast, the rail base on the field side moves down, which reduces the deflection of the clip and induces smaller clamping forces.

As shown in Figure 9, five linear potentiometers were used in the test to measure the displacement of the rail. A comparison between the output of the FE model and the test measurements on the rail displacement is shown in Figure 15. For vertical displacements of the rail base, a positive measurement indicates that the rail base was lifted up; and for lateral displacements of the railhead, a positive measurement indicates that the rail was pushed towards the field side. Some comparisons between model outputs and test measurements are shown as examples. Figure 15 illustrates that the field side of the rail base moves downward due to the lateral load, and the railhead moves towards the field side. Due to the 10 kN (2.2 kips) lateral load applied at the rail web, the vertical displacement of the rail base at the field

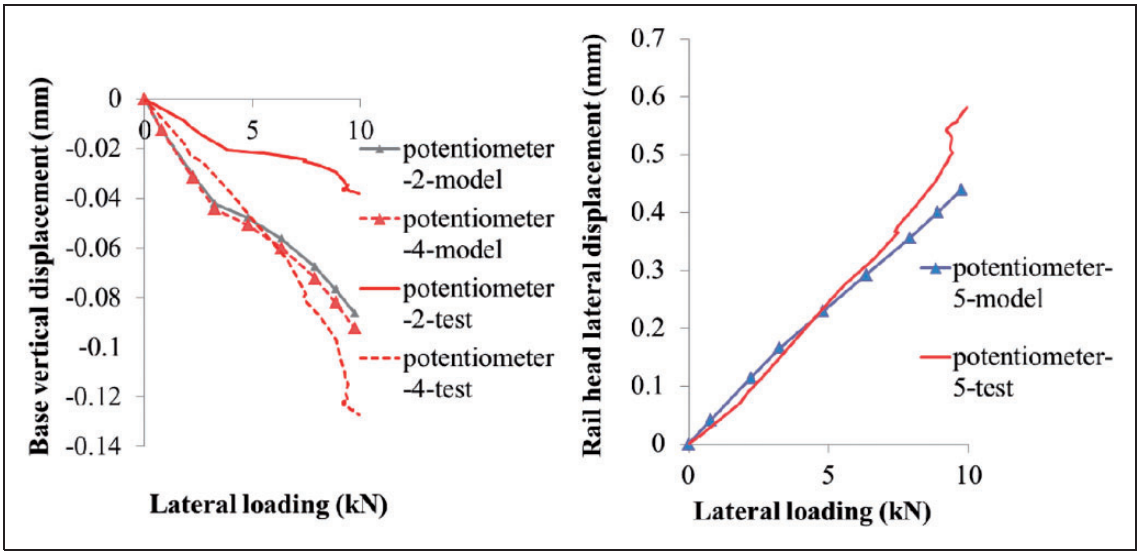

Figure 15. Comparison of model and test values of the vertical displacement of the rail base and the lateral displacement of the railhead. (a) Potentiometer 2 and 4, and (b) Potentiometer 5.

side is about 0.1 mm (0.004 inch) and the lateral displacement of the railhead is about 0.6 mm (0.024 inch). A negative displacement can be observed at potentiometer 2 and potentiometer 4, and a positive displacement can be observed at potentiometer 5. It is clear that the two displacements measured at the field side vary. As the positions of potentiometer 2 and potentiometer 4 are approximately symmetric in the longitudinal direction about the loading point, the difference in test measurements indicates a possible difference in the installation of the potentiometers.

The output of the FE model shows a smaller displacement than that of the test measurement at all three positions, which indicates a larger rotation of the rail was observed in the test. Possible sources of the difference includes the material property definition of the rail pad and the abrasion plate, as the material properties of the raw materials were used in the model, and further material treatment in the process of manufacturing was not considered in the model.

As illustrated by the results presented in this section, there was a good agreement between what was observed in the FE model and test results in terms of the vertical strain of the rail, the surface strain of the rail clip, and the displacements of the rail. Although the magnitude of the applied load in the experiment was relatively low compared with that of a field loading scenario, the objective was to compare and validate the FE model of the fastening system in the elastic stage under lateral loading. In the future, a vertical load will be introduced into the laboratory experiment along with a more comprehensive FE model that simulates the structural behavior of the concrete sleeper. Field experiments will also be used for further model validation.

Parametric study

The validated FE model was utilized to look into the system behavior under different loading scenarios. Under working conditions, the wheels of vehicles apply both vertical and lateral loads to the rail through the contact patch on the top and lateral surfaces of the railhead. On curved track, the loading condition can generally be characterized with the ratio between lateral and vertical load (L/V ratio). The loading combination was designed based on the loading environment expected in North American low-speed (speed lower than 64.4 km/h (40 mile/h)) mainline freight segment. The distribution of loading between concrete sleepers at a spacing of 0.483 m (19 inch) was assumed. The ratios between lateral and vertical loadings considered in the model were 0.25, 0.375 and 0.5.[1] The load environment specified in the AREMA manual for curved track under low-speed mainline freight traffic indicates an L/V ratio of 0.25 for the wheel load,[1] however, considering the distribution of the vertical and lateral loads among multiple rail seats, an L/V ratio higher than 0.25 should be expected at a single rail seat. After pre-stressing and clamping forces were applied, a vertical load of 133 kN (30 kips) was applied on the top of the railhead as a pressure over an area of 64.5 mm^2 (0.1 $inch^2$). Afterwards, a lateral loading based on the L/V ratio was applied on a small area of the lateral surface of the railhead. The boundary condition in the FE model remained the same as in the validated model.

Results of the parametric study

Stress analysis. The maximum tensile and compressive stresses of the components of the fastening system under different loading scenarios are summarized

in Table 3. To eliminate the effect of a geometric singularity, the extreme stress output of a concrete element was calculated by averaging the maximum tensile and compressive stress outputs of surrounding nodes. As the stress distributions among the three L/V ratios are similar, only the cases with L/V ratios of 0.25 and 0.5 are listed to show the range of stress values. In addition, a plan view of the compressive stress contours of the concrete is shown in Figure 15, where the holes on the surface indicate the positions of the shoulder inserts. A compressive stress concentration was observed in the concrete around the insert of a shoulder. This stress concentration is due to a combination of the clamping force and lateral loading, and based on the stress contour the concrete it was already crushed. In Figure 16 it can be observed that the compression zone under the abrasion plate also shifted to the field side due to the rotation of the rail. A high tensile stress is observed between the two shoulder inserts, a result of lateral loading and the concrete already being cracked. Due to geometric and confinement effects, the concrete was able to reach compressive stresses higher than its peak strength.

Deflection analysis. The lateral resistance of the rail consists of several parts: the friction between rail and rail pad, the lateral component of the uneven clamping force, and the normal interaction force transferred through the insulator when the gap between the insulator and shoulder is closed. The displacements of the railhead and rail base under vertical and lateral loads are important criteria as they determine the support condition of the wheel. The displacements of the rail under vertical and lateral loadings are a combination of translation and rotation: the clamping force from the clips acts as the resistance for rotation and the friction between rail and rail pad acts as the resistance for translation.

Figure 17 shows the relationship between the lateral load and the lateral displacements of the railhead and the rail base. For track alignment The FRA's Track Safety Compliance Manual[14] requires that on curved track of class 5 track the deviation of the mid-ordinate from a 9.4-m (370 inch) chord may not be more than 0.0127 m (0.5 inch). It was observed that the lateral displacement of the railhead was smaller than 0.0127 m (0.5 inch) until the lateral loading reached 57.8 kN (13 kips). As the material of the

Table 3. Maximum tensile and compressive stress of components under different loading scenarios.

Component	Maximum compressive Stress (MPa)		Yielding strength or fc' (MPa)	Maximum tensile Stress (MPa)		Yielding or cracking Strength (MPa)
	L/V = 0.25	L/V = 0.5		L/V = 0.25	L/V = 0.5	
Concrete	30	70.3	48.3	1.7	5.5	5.5
Clip	1271.9	1475.5	1261.8	1160.3	164.5	1261.8
Rail	170.2	277.5	1034.3	95.5	219.3	1034.3
Insulator	130.8	121.1	64.1	74.2	101	64.1
Rail Pad	26.6	49.4	8.3	0.8	9.3	8.3
Abrasion Plate	25.6	46.1	64.1	2.3	8.6	64.1

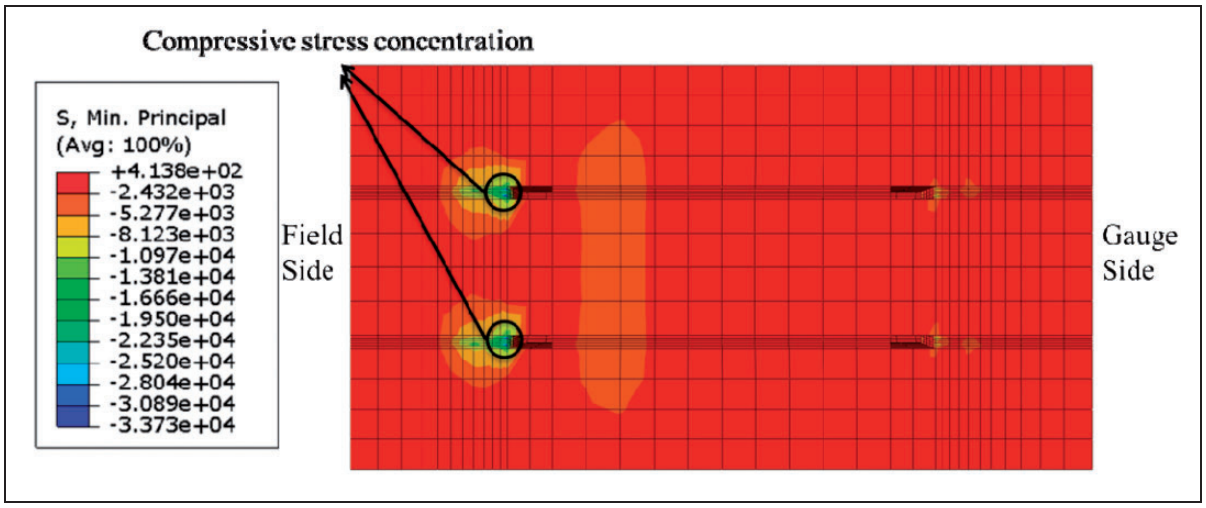

Figure 16. Concrete compressive stress contour in psi ($L/V = 0.5$, unit: psi. 1 psi = 6.89 kPa).

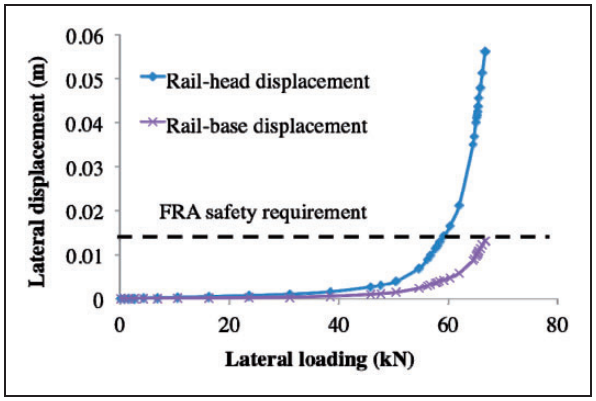

Figure 17. Relationship between lateral loading and lateral displacement of the rail.

field-side insulator had already yielded, the lateral displacement of the railhead increased more rapidly afterwards. The numerical result justifies the field practice of using a stiffer insulator on the field side. It is also required that the base of the rail should not move laterally more than 0.0127 m (0.5 inch) relative to the sleeper, and the output of the model is within the acceptable range. As the gap between the insulator and the shoulder in the model was relatively small, it was soon closed after the application of the lateral loading. As a result, the shoulder prevented any further sliding of the rail, and therefore the dominant mode of displacement became rotation. Any further lateral displacement of the rail base was due to the deformation of the insulator post and/or shoulder.

It is important to note that in this model, the lateral bending stiffness of the rail was ignored due to the support condition on the ends of a rail segment not being simulated. With this limitation, the lateral displacement of the rail was overestimated in this model.

Conclusions

In this paper, a detailed 3D FE model for a sleeper and fastening system was presented. The FE model consisted of a concrete sleeper and fastening system based on actual product designs, and was loaded through practical static loadings after a pre-stressing action was applied. Inelastic material properties, as well as component tangential and normal interactions, were incorporated into the model. The 3D FE model was validated using a laboratory test conducted at the University of Illinois at Urbana-Champaign. Good agreement was observed between the model output and the test measurement. After the validation, the 3D FE model was used to simulate the effects of different loading scenarios. Three loading scenarios were considered in the analysis ($L/V = 0.25,\ 0.375,\ 0.5$). The conclusions drawn from this study are now summarized.

1. A compressive stress concentration was observed around shoulder insert and it resulted in the crushing of the concrete. At the same time a tensile stress concentration was observed between the two inserts of the shoulder leading to cracking of the concrete. This suggests a potential risk of a shoulder pull-out failure of the fastening system under repeated wheel loads.
2. Under an L/V ratio of 0.5, yielding of the components was observed in the clip, the insulator and the rail pad.
3. The lateral displacement of the railhead satisfied the FRA safety requirement until the lateral loading reached 57.8 kN (13 kips). Severe yielding was observed on the field-side insulator whereas deformation in the gauge-side insulator was smaller. This observation justifies the field practice of using a stiffer insulator on the field side. The dominant displacement mode of the rail was rotation, and the lateral displacement of the rail base was within the acceptable range even under an L/V load ratio of 0.5.

The functionality of the model of the pre-stressed concrete sleeper and fastening system can be further improved by replacing the concrete block with a full-scale concrete sleeper to simulate the structural behavior of the sleeper. In addition, the rail behaving as a continuous beam supported by multiple sleepers can also be incorporated into the FE model to evaluate the distribution of vertical and lateral wheel loads. These improvements will be implemented in future models so as to better simulate the sleeper/fastener system under different loading scenarios. More laboratory and field experiments are required to further validate the FE model under more realistic loading scenarios. The validated FE model can be used for virtual experiments and further parametric studies that may focus on the effects of design parameters (e.g. sleeper spacing, sleeper length, material property, etc.) on critical output parameters related to track safety such as rail-seat stress distribution, railhead displacement and yielding of fastening system components.

Funding

The authors would like to express their sincere gratitude to the United States Department of Transportation (US DOT) FRA for providing funding for this research project. The published material in this paper represents the position of the authors and not necessarily that of the DOT.

Acknowledgements

The authors want to thank Jose Mediavilla (Amsted RPS), and Pelle Duong (CXT Concrete Ties) for providing product information and advice that proved invaluable to this work.

References

1. American Railway Engineering and Maintenance-of-Way Association. Ties. In: *Manual for railway engineering*. Lanham, MD: American Railway Engineering and

Maintenance-of-Way Association, 2010, pp.30-4-20–30-4-24.
2. Fröhling RD. Low frequency dynamic vehicle/track interaction: modelling and simulation. *Veh Syst Dyn* 1998; 29: 30–46.
3. Yu H, Jeong D, Choros J and Sussmann T. Finite element modeling of prestressed concrete cross tie with ballast and subgrade support. In: *The ASME 2011 international design engineering technical conference & Computers and information in engineering conference,* Washington DC, 29–31 August 2011. NY, USA: ASME.
4. Yu H and Jeong DY. Finite element modeling of railroad concrete cross ties - a preliminary study. In: *The international conference on railway engineering,* Beijing, China, 20–21 August 2010. Beijing, China: China Railway Publishing House.
5. Dahlberg T and Lundqvist A. Load impact on railway track due to unsupported sleepers. *Proc IMechE, Part F: J Rail Rapid Transit* 2005; 219: 67–77.
6. Remennikov AM and Kaewunruen S. Investigation of free vibrations of voided concrete sleepers in railway track system. *Proc IMechE, Part F: J Rail Rapid Transit* 2007; 221: 495–507.
7. Abrishami HH and Mitchell D. Bond characteristics of pretensioned strand. *ACI Mater J* 1993; 90: 228–235.
8. González-Nicieza C, Álvarez-Fernández MI, Menéndez-Díaz A, et al. Failure analysis of concrete sleepers in heavy haul railway tracks. *Engng Fail Anal* 2008; 15: 90–117.
9. Rezaie F, Shiri MR and Farnam SM. Experimental and numerical studies of longitudinal crack control for prestressed concrete sleepers. *Engng Fail Anal* 2012; 26: 21–30.
10. Kaewunruen S and Remennikov AM. Nonlinear transient analysis of a railway concrete sleeper in a track system. *Int J Struct Stab Dyn* 2008; 8: 505–520.
11. Dassault Systemes Simulia Corp. ABAQUS analysis user's manual, Version 6.11, 2011.
12. Kernes RG, Edwards JR, Dersch MS, et al. Investigation of the dynamic frictional properties of a concrete cross tie rail seat and pad and its effect on rail seat deterioration (RSD). In: *The 91st annual meeting of the Transportation Research Board*. Washington DC, 22–26 January 2012. Washington DC, USA: Transportation Research Board.
13. Yamaguchi Y. *Tribology of plastic materials: their characteristics and applications to sliding components*. Philadelphia, USA: Elsevier, 1990, p.362.
14. Federal Railroad Administration. Track safety standards classes 1 through 5. In: *The Federal Railroad Administration track safety standards compliance manual*. Washington DC: Federal Railroad Administration, 2007.